scientific reports

Check for updates

OPEN

Chitosan/ZnO nanohybrid as an efficacious compatibilizer for PLA/PBS blend suitable candidate for biodegradable packaging applications

Parsa Dadashi[2,3], Rozgol Bonsale[1,3] & Amir Babaei[1]✉

In this study, chitosan–zinc oxide (CS-ZnO) nanohybrids were investigated as a new compatibilizer for biodegradable poly(lactic acid)/poly(butylene succinate) (PLA/PBS) blends. The novelty of this work lies in the synergistic effect arising from the hybridization of ZnO with chitosan, which enhances the interfacial compatibility between PLA and PBS and overcomes the limitations of pure ZnO, such as agglomeration and weak adhesion to the polymer matrix. PLA/PBS blends (80/20 wt%) were reinforced with different concentrations (0.1–0.5 wt%) of ZnO and CS-ZnO via solution casting. Mechanical testing showed that the addition of only 0.25 wt% of CS-ZnO improved the elongation at break by 50% and the tensile strength by 52% compared to pure ZnO. Morphological analysis using scanning electron microscopy (SEM) showed that the addition of only 0.25 wt% of CS-ZnO into PLA/PBS decreased the radius of PBS droplets from 423 nm to 349 nm, indicating improved compatibility between the PLA and PBS phases. This compatibility was further supported by rheological measurements, which showed an increased viscosity in the nano-hybrid-filled blend from 50 Pa.s to 110 Pa.s. Hydrolytic degradation tests, evaluated through mass loss over time, revealed accelerated degradation in CS-ZnO nanocomposites, because of increased hydrophilicity and interfacial areas. This study employed Density Functional Theory (DFT) with the semi-empirical PM6 method to estimate binding energies in binary and ternary systems, confirming experimental findings. Strong negative binding energies for PLA–ZnO and PBS–ZnO suggest high interfacial affinity, while PLA–CS showed weakly unfavorable interactions. The addition of ZnO to PLA–CS and PBS–CS systems resulted in favorable binding energies, emphasizing CS-ZnO hybrids' role in improving compatibility, stability, and bioactivity-controlled degradability of PLA/PBS-based nanocomposites, advancing sustainable materials for packaging and biomedical applications.

Keywords Biodegradable, Bio-Packaging, Rheology

In recent years, the demand for environmentally friendly and sustainable materials has sparked significant interest in biodegradable polymers, which are typically derived from renewable resources[1–3]. Among these, polylactide (PLA) and poly(butylene succinate) (PBS) have achieved considerable attention due to their biodegradability, commercial availability, and favorable mechanical and thermal properties[4,5]. However, each material has inherent limitations that restrict its standalone applications[4–6]. While exhibiting high strength and stiffness, PLA is known for its brittleness, low heat resistance, and slow crystallization rate, limiting its performance in flexible and thermally demanding applications[7,8]. Conversely, PBS exhibits excellent flexibility and thermal stability, but lacks the mechanical rigidity and processability that are offered by PLA[7,8].

To overcome these shortcomings, blending PLA with PBS has emerged as a promising strategy for developing materials with balanced mechanical, thermal, and degradation performances[9–12].

[1]Department of Polymer Engineering, Faculty of Engineering, Golestan University, Gorgan 15759-49138, Iran. [2]Advanced Polymer Materials & Processing Lab, School of Chemical Engineering, College of Engineering, University of Tehran, Tehran 14174- 66191, Iran. [3]These authors contributed equally: Parsa Dadashi and Rozgol Bonsale. ✉email: a.babaei@gu.ac.ir

However, the incompatibility between PBS and PLA causes poor adhesion and a weak interface between the two polymers, preventing the achievement of synergistic effects from blending. To improve the adhesion between these two biodegradable polymers, it is important to use an appropriate component that acts as a compatibilizer, which should possess biocompatibility to make the blend suitable for packaging applications.

Chitosan (CS), a natural polysaccharide derived from chitin, is highly valued for its biocompatibility and biodegradability. As a result, interest in developing CS/polymer composites has increased[13–19]. Furthermore, CS can serve as a compatibilizer for PLA and PBS owing to its functional groups. To enhance the compatibility and interaction between CS and the PLA/PBS matrix, CS can be functionalized or hybridized. Such modifications not only enhance interfacial adhesion but can also promote faster degradation, improve mechanical stability during use, and enhance barrier properties, thereby expanding the potential for industrial applications of PLA/PBS blends. Zinc oxide (ZnO), which can influence hydrolytic degradation, can be considered a good candidate for hybridization with CS[20–22]. Studies show that adding ZnO to PLA improves mechanical strength and biodegradation, making it more suitable for advanced applications such as food packaging[23]. On the other side, the hybridization of ZnO with chitosan offers a promising strategy to overcome the thermal degradation challenges associated with PLA. This approach not only stabilizes ZnO during melt processing but also enhances the overall thermal and mechanical properties of the composite material.

Despite these advances, limited understanding remains regarding the molecular-level interactions between CS-ZnO and PLA/PBS phases, and how these interactions govern the composite's macroscopic behavior. Addressing this knowledge gap is crucial for the rational design of next-generation biodegradable materials.

In this study, we employ a multiscale characterization framework combining experimental analyses—such as rheology, hydrolytic degradation, and microstructure evaluation—with density functional theory (DFT) simulations to elucidate the interfacial mechanisms governing the performance of PLA/PBS/CS–ZnO composites. This integrated approach clarifies how the incorporation of CS/ZnO affects mechanical reinforcement and degradation kinetics throughout the bulk material. The findings provide predictive insights for the design of sustainable biopolymer nanocomposites with tailored functional properties, supporting the global transition toward a circular and eco-efficient materials economy.

Experimental part

Materials and methods

Materials

In the present study, polylactic acid (PLA) polymers (2003D) with a melt flow index of 6 g/10 min and a molecular weight of 200,000 g/mol were procured from NatureWorks (USA).

Polybutylene succinate (PBS) used in this study was a collaborative commercial endeavor of PTT (PTT GC41), Mitsubishi Chemical Corporation (MCC), and Global Chemical Corporation. This particular PBS variant exhibits a melt flow index of 4 g/10 min and possesses a molecular weight of 1000 g/mol.

For the synthesis of zinc oxide (ZnO) nanoparticles, the required reagents were procured from Sigma-Aldrich Chemical Co. (USA). These reagents include zinc acetate, glacial acetic acid (≥ 99.85% purity), and sodium hydroxide (NaOH) at a purity of 98%.

Two different types of chitosan were used to synthesize the ZnO-chitosan nanohybrid. The chitosan (CS) powder, with a low molecular weight of 50,000–80,000 Da and 85% deacetylation degree, was obtained from Aldrich Sigma Company. Chitosan nanofibrils were also prepared by Nano Novin Polymer Co. in Iran.

Synthesis of ZnO-NPs

ZnO nanoparticles were synthesized using an in-situ synthesis procedure as described in the previous literature[20].

First, 40 milliliters of 1 M zinc acetate solution was added to 60 milliliters of deionized water. Then 100 milliliters of 0.5 M sodium hydroxide solution were added drop by drop to the prepared solution with an ultrasonic homogenizer (140 watts, UP400St, Hielscher, Germany) to achieve a light milky solution.

After 120 min of vigorous stirring at room temperature, the obtained light milky suspension of ZnO NPs was sonicated for 20 min. The solution was centrifuged and washed several times with deionized water to remove the excess zinc acetate and other soluble impurities. Afterward, the obtained solution was dried using a freeze dryer (Beta2-8 LD plus; Christ Co. Germany) at −40 °C for 48 h and finally characterized. A schematic of the synthesis of ZnO-NPs can be observed in Fig. 1**(a).**

Synthesis of nano-fibrillar chitosan-ZnO hybrid

In the present study, both chitosan powder and chitosan fibrils were utilized for the synthesis of chitosan-ZnO nanoparticles hybrid[20].

A nanohybrid of nano-fibrillar chitosan-ZnO (NF-CS-ZnO) was prepared using a simple and rapid sono-coprecipitation technique in two steps.

First, 55 ml of nano-fibrillar chitosan was dispersed in a 1 M solution of zinc acetate dihydrate under a magnetic stirrer (400 rpm) at room temperature to achieve a homogeneous suspension.

Following the first step, 25 ml solutions containing 1 M sodium hydroxide were added dropwise to the above solution under an ultrasonic homogenizer (200 W, 150% amplitude) until the pH of the mixture reached 7.

Afterward, the milky light suspension was continuously stirred for 2 h at 80 °C.

Finally, similar to the synthesized ZnO NPs, the resulting suspension containing NF-CS-ZnO-NPs hybrid was centrifuged and washed several times with deionized water to eliminate soluble impurities. Then, it was dried using freeze-drying at −40 °C for 48 h. The process of synthesizing NF-CS-ZnO-NPs can be observed in Fig. 1(b).

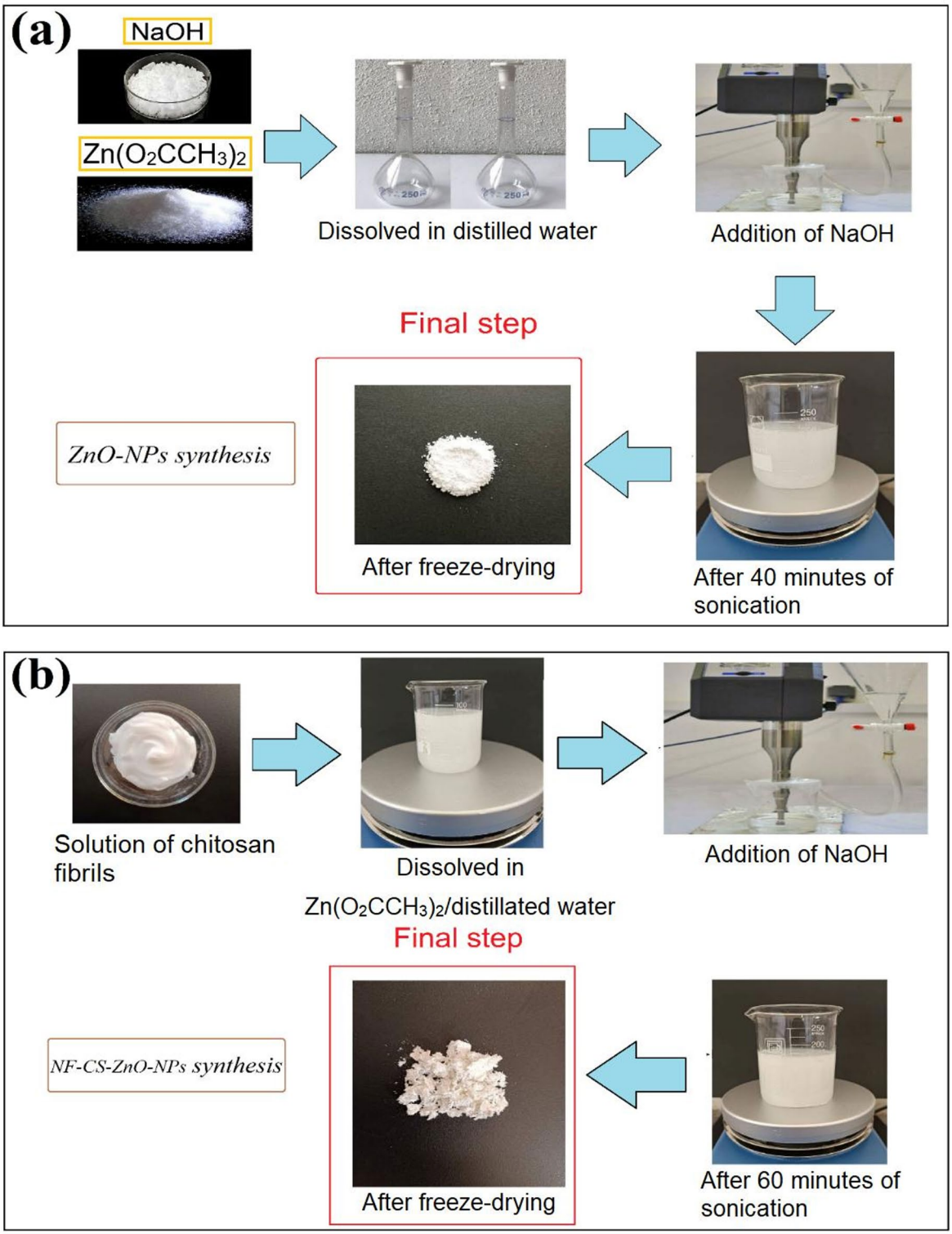

Fig. 1. Schematic of sample preparations: (**a**) ZnO-NPs synthesis, and (**b**) NF-CS-ZnO-NPs nanocomposites.

Synthesis of powder chitosan-ZnO nanohybrid

The process for synthesizing the powder chitosan-ZnO (P-CS-ZnO) nanohybrid was completed as follows: In the first step, 1.5 g of chitosan powder was dissolved in 1.5 mL of 1% acetic acid and 150 mL of deionized water at room temperature.

In the second step, 40 mL of a 1 M zinc acetate solution was added to the above-mentioned solution under a magnetic stirrer (400 rpm) at ambient conditions.

Following the second step, 120 mL of 1 M sodium hydroxide solution was added dropwise under ultrasonic homogenizer conditions (160 watts, 200% amplitude) at room temperature.

The obtained P-CS-ZnO-NPs were stirred for 2 h at 80 °C and then washed multiple times with deionized water to remove impurities, similar to the NF-CS-ZnO-NPs hybrid.

Eventually, the P-CS-ZnO-NPs hybrid was dried using freeze-drying at −40 °C for 24 h.

Preparation of nanocomposite films

In this study, nanocomposites were fabricated using the solvent casting method. The solvent used in this process was dimethylformamide (DMF), which was purchased from Kimia Arian Company. To prepare the samples, specific amounts of polylactic acid and polybutylene succinate in a ratio of (20/80) were dissolved in the mentioned solvent. The resulting mixture was stirred at 70 °C for 2 h to ensure complete dissolution.

On the other hand, predetermined amounts of each type of nanomaterial were completely dissolved in a specific amount of solvent based on their weight in grams. These solutions were then fully dispersed using an ultrasonic probe for 5 min at a power of 100 watts. The obtained suspension was subsequently added to the polymer solution and partially mixed using a magnetic stirrer. The prepared polymer solution was also subjected to ultrasonic probe treatment for 8 min at 100 watts to achieve uniform nanomaterial dispersion.

For film preparation, the final mixture was poured into a 10 cm diameter silicone mold and dried in an oven at 80 °C for 8 h. All nanocomposites examined in this research, containing different percentages of zinc oxide nanoparticles and chitosan-zinc oxide hybrids, were fabricated using this method. The prepared nanocomposites were named according to Table 1.

Characterization methods

FT-IR analysis

The analysis of functional groups in the chemical structure of the prepared samples was conducted using the RX infrared spectroscopy device from PerkinElmer Inc., USA, at the Central Laboratory of Golestan University. For sample preparation and testing, tablets were made from synthesized nanoparticle powders mixed with KBr salt. The test was performed using the device in the range of 400–4000 cm^{-1}, and the results were evaluated and analyzed.

UV-Vis analysis

In this study, the shift of characteristic peaks of zinc oxide nanoparticles and chitosan-zinc oxide hybrids was analyzed using the PG Instruments UV-Vis spectrophotometer, model T90+, at the Central Laboratory of Golestan University. The analysis was conducted within the wavelength range of 190–450 nm.

FE-SEM analysis

To observe and analyze the morphology of zinc oxide nanoparticles, chitosan-zinc oxide nanohybrids, and the prepared films, a scanning electron microscope (SEM) was used. The surface of all mentioned samples was coated with gold and then placed under vacuum in the SEM.

The morphology analysis of zinc oxide nanoparticles and chitosan-zinc oxide nanohybrids was performed using the field emission scanning electron microscope (FE-SEM) TESCAN MIRA3-XMU at the Razi Metallurgy Research Center. Additionally, the analysis of the prepared films was carried out using the SERONTECHNOLOGIES AIS2100 scanning electron microscope.

Rheometry analysis

Rheometry testing demonstrates the rheological properties (the study of polymer behavior in the molten state) of polymeric materials. The rheological properties of PLA/PBS nanocomposites containing ZnO nanoparticles and chitosan-zinc oxide nanohybrids were examined using rheometry testing. This test was conducted using an Anton Paar MCR 501 rheometer with parallel plates. Additionally, all tests were performed at 190 °C in an oscillatory mode between two parallel plates within a frequency range of 0.01–620 rad/s under a nitrogen atmosphere. To obtain results within the linear viscoelastic region, a strain amplitude of 1% was considered.

Sample code	PLA (wt%)	PBS (wt%)	ZnO (wt%)	NF-ZnO-CS-NPs (wt%)	*P*-ZnO-CS-NPS (wt%)
PLA/PBS	80	20	0	0	0
ZnO 0.1	80	20	0.1	0	0
ZnO-CS-F 0.1	80	20	0	0.1	0
ZnO-CS-F 0.25	80	20	0	0.25	0
ZnO-CS-F 0.5	80	20	0	0.5	0
ZnO-CS-P 0.1	80	20	0	0	0.1
ZnO-CS-P 0.25	80	20	0	0	0.25
ZnO-CS-P 0.5	80	20	0	0	0.5

Table 1. Composition of samples used in this study.

Tensile test

To measure the mechanical properties of polylactic acid/polybutylene succinate nanocomposites containing zinc oxide nanoparticles and chitosan-zinc oxide nanohybrids, a tensile or stress-strain test was conducted in accordance with ASTM D638 standard at a constant temperature of 25 °C. The test was performed using the GOTECH AI-3000 device.

During the test, all samples, each with a length and width of one centimeter, were stretched at a constant speed of 10 mm/min. Additionally, to minimize testing errors, five strips were prepared for each sample, and the final results were reported as the average of their measurements.

Hydrolytic degradation

The hydrolytic degradation of the prepared samples was studied by immersing all films, with identical and specified dimensions, in separate containers containing 10 mL of 1 M sodium hydroxide at room temperature. After 42 h, their weight changes were examined. At the end of the predetermined duration, the samples were removed from the 1 M sodium hydroxide solution, thoroughly washed with distilled water, and completely dried to assess their weight changes. After evaluating the weight loss compared to the initial weight, the results were plotted in a graph based on nanoparticle concentration. Additionally, photographs of all samples were taken after the test to visually observe the extent of degradation.

DFT calculation

Inorderto theoretically study the molecular interactions among PLA, PBS, CS, and ZnO nanoparticles, quantum chemical calculations were carried out using the Gaussian software package. All structures were geometrically optimized using the PM6 semi-empirical method, which provides a suitable balance between computational efficiency and accuracy for large polymeric and hybrid systems. The calculations were performed at the ground state with zero net charge and singlet spin multiplicity, under default convergence criteria.

The binding energy (ΔE_{bind}) for each complex was calculated using Eq. 1.

$$\Delta \mathrm{E}_{bind} = E_{complex} - \sum E_{individual\ components} \tag{1}$$

where $E_{complex}$ is the total electronic energy of the optimized complex (e.g., PLA–ZnO), and the $E_{individual\ components}$ are the total energies of the separately optimized species (e.g., PLA and ZnO). All energies were reported in atomic units (a.u.) and converted to kJ/mol where appropriate. Negative values of ΔE_{bind} indicate thermodynamically favorable interactions and greater complex stability.

These results were used to interpret and support experimental observations, including mechanical performance, morphological dispersion, rheological relaxation, and hydrolytic degradation. The strong negative binding energies in PLA–ZnO and PBS–ZnO complexes corroborate the improved interfacial adhesion and stability observed in nanocomposites, while moderate stabilization in ternary systems, such as PLA–CS–ZnO, suggests that ZnO facilitates compatibility between polymers with inherently weak affinity, such as PLA and chitosan.

Result and discussion

Validation of the synthesis of ZnO-NPs, P-CS-ZnO-NPs, and F-CS-ZnO-NPs

FTIR results

Figure 2(a) presents the FTIR spectra of ZnO-NPs, CS, and the P-CS-ZnO-NPs nano-hybrid, recorded in the range of 400–4000 cm^{-1}. As the infrared spectra of ZnO-CS-NPs hybrids with different morphologies are identical, only the P-CS-ZnO-NPs spectrum as representative was shown.

For the case of ZnO-NPs, a characteristic absorption peak at 450 cm^{-1} is seen which corresponds to the Zn–O stretching mode, while a broad peak at 3400 cm^{-1} is attributed to the –OH group stretching vibrations. Besides, a broad peak centered at approximately 1550 cm^{-1} indicates adsorbed water molecules on the ZnO-NPs surface[24]. Additionally, a peak at 1400 cm^{-1} is associated with the vibrational mode of CO_2 adsorbed from the atmosphere[25].

For the pure CS, a broad absorption peak at 3440 cm^{-1} arises from the stretching vibrations of $–NH_2$ and –OH groups[26]. Peaks at 2861 cm^{-1}, 2922 cm^{-1}, 1653 cm^{-1}, 1080 cm^{-1}, and 1429 cm^{-1} are assigned to the stretching vibrations of $–CH_2$, $–CH_3$, C = O, and –C–O–C groups, and the scissoring vibrations of $–NH_2$ groups, respectively[27].

The P-CS-ZnO-NPs nano-hybrid exhibits characteristic peaks at 3450 cm^{-1}, 2910 cm^{-1}, 1650 cm^{-1}, 1380 cm^{-1}, and 1080 cm^{-1}, corresponding to the stretching vibrations of –OH, $–CH_2$, C = O, and –C–O–C groups, and the scissoring vibrations of $–NH_2$ groups, respectively. A prominent peak at 430 cm^{-1}, attributed to the O–Zn–O stretching mode, confirms the presence of ZnO within the nano-hybrid structure[20]. Compared to pure CS, the P-CS-ZnO-NPs spectrum shows increased peak intensity and a shift to lower wavenumbers in the 1550–1700 cm^{-1} range, likely due to interactions between the amine ($–NH_2$) groups of CS and the hydroxyl (–OH) groups of ZnO-NPs, which is in consistent with the previous studies[27–29].

UV-Visible results

Figure 2(b) displays the UV-Vis absorption spectra of ZnO-NPs, P-CS-ZnO-NPs, and NF-CS-ZnO-NPs nano-hybrids, normalized to account for concentration effects. Pure CS exhibits no absorption peak due to the absence of conjugated double bonds in its molecular structure[30]. In contrast, ZnO-NPs show a broad absorption peak at 223 nm, attributed to the electron transitions from the valence band to the conduction band, as it is frequently reported[31].

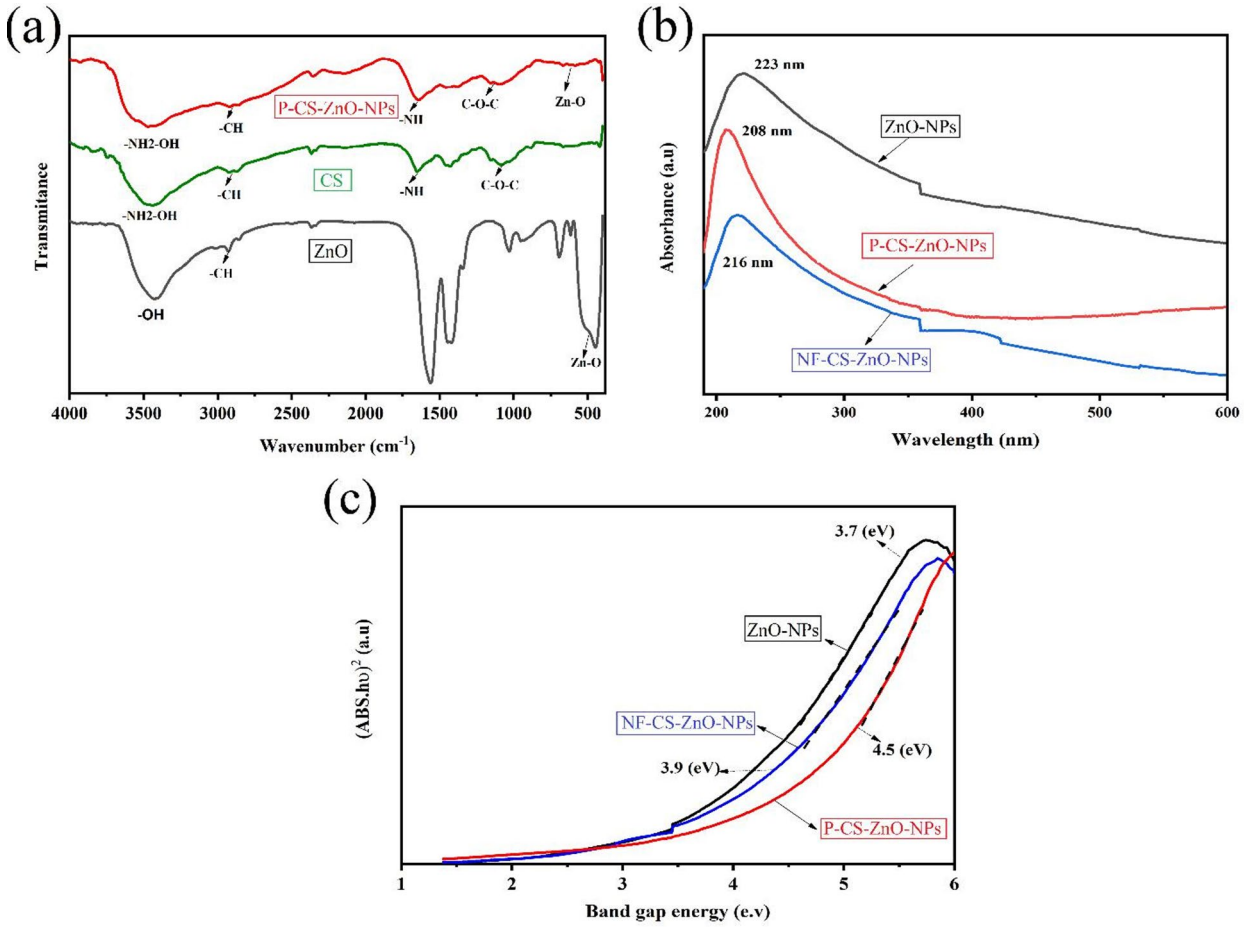

Fig. 2. Plots illustrating (**a**) the FT-IR spectra of ZnO nanoparticles, CS, and P-CS-ZnO NPs; (**b**) the UV–Vis absorption spectra of ZnO nanoparticles, P-CS-ZnO NPs, and NF-CS-ZnO NPs nanohybrids; and (**c**) the corresponding energy band gaps of ZnO nanoparticles, P-CS-ZnO NPs, and NF-CS-ZnO NPs nanohybrids.

Decoration of ZnO-NPs with CS resulted in a blue shift for the P-CS-ZnO-NPs and NF-CS-ZnO-NPs nano-hybrids, with sharp, narrow absorption peaks at 208 nm and 216 nm, respectively. This shift aligns with Kubo's theory, which suggests that the UV absorbance of ZnO nanoparticles is size-dependent, a correlation supported by prior studies[31–33]. The blue shift and peak narrowing suggest a homogeneous dispersion of smaller, uniformly sized ZnO nanoparticles within the chitosan (CS) matrix, driven by strong interactions between ZnO-NPs and CS chains. This observation is consistent with the non-agglomerated structure, as further confirmed by the SEM analysis, where CS appears to stabilize and direct the formation of ZnO nanoparticles.

Bandgap energies for ZnO-NPs, NF-CS-ZnO-NPs, and P-CS-ZnO-NPs nano-hybrids were calculated using the Kubelka–Munk equation, plotting $(\alpha h\nu)^2$ against photon energy ($h\nu$), as shown in Fig. 1(c). The bandgap energies are 3.7 eV, 3.9 eV, and 4.5 eV, respectively. The increased bandgap in CS-ZnO nano-hybrids, particularly NF-CS-ZnO-NPs, compared to ZnO-NPs, indicates the formation of smaller ZnO nanoparticles in the presence of CS[34,35].

FE-SEM

The morphology and microstructure of ZnO-NPs, NF-CS-ZnO, and P-CS-ZnO nano-hybrids were characterized using FE-SEM, with micrographs presented in Fig. 3. The ZnO-NPs exhibit a rod-like morphology with thicknesses ranging from 278 to 393 nm (Fig. 3(a)). In contrast, FE-SEM images of NF-CS-ZnO and P-CS-ZnO nano-hybrids (Fig. 3(b) and 3(c)) reveal rod-like ZnO-NPs uniformly distributed across the CS substrate.

It can be seen that, hybridization with CS significantly reduced ZnO-NP aggregation, yielding smaller particles (25–30 nm) in both NF-CS-ZnO and P-CS-ZnO nano-hybrids. This is attributed to CS role acting as a steric barrier, preventing ZnO seed aggregation during growth, consistent with prior studies[27,34,36] Additionally, ultrasound during synthesis further minimizes ZnO-NP agglomeration[20].

Notably, NF-CS-ZnO nano-hybrids display a more even uniform distribution and smaller ZnO-NPs compared to P-CS-ZnO nano-hybrids. This difference is likely due to two factors: (1) higher surface area of fibrillar CS and complex morphology, which enhance the interaction with ZnO precursors and improve nucleation and growth control, and (2) the fibrous structure of fibril CS, which physically entraps or sterically hinders ZnO-NPs, preventing agglomeration and promoting smaller particle sizes.

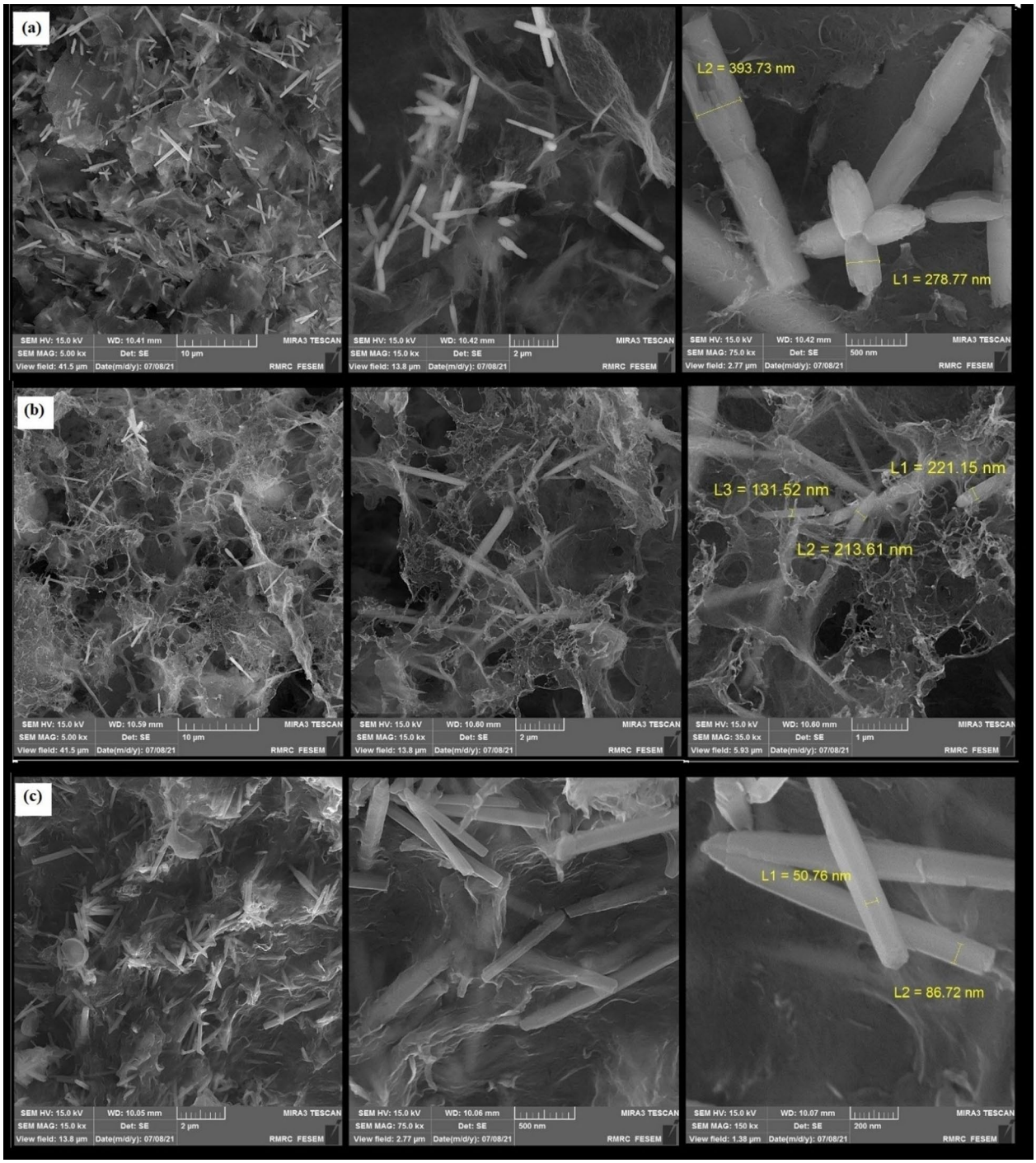

Fig. 3. FESEM of (**a**) ZnO-NPs, (**b**) NF-CS-ZnO nanohybrids, (**c**) P-CS-ZnO nanohybrids.

These findings align with UV-Vis absorption results, which indicate smaller ZnO-NPs in CS-fibril hybrids (rod lengths of 50–80 nm), further evidencing well-dispersed nanoparticles. Thus, the structural properties of fibrilar CS facilitate the formation of smaller, more uniformly distributed ZnO-NPs compared to powdered CS.

PLA/PBS nano-hybrid composites results

Morphological evaluation of PLA/PBS nanocomposites

The distribution and localization of nanoparticles depends on the interfacial tension of each component, and it can be calculated using the wetting coefficient and Young's equation (Eq. 2) as follows[37]:

$$\omega_{12} = cos\theta = \frac{\gamma_{s2} - \gamma_{s1}}{\gamma_{12}} \quad (2)$$

Sample	γ^d (mNm^{-1})	γ^p (mNm^{-1})	γ_s (mNm^{-1})	Reference
PLA	37	16.5	53.5	[38]
PBS	39.9	8.7	48.6	[38]
ZnO	18.5	32	40.5	[39]

Table 2. Surface tension of PLA, PBS, and ZnO-NPs.

Sample 1	Sample 2	Interfacial tension(mNm^{-1})	Code
PLA	PBS	2.58	γ_{12}
PLA	ZnO	3.58	γ_{1s}
PBS	ZnO	7.12	γ_{2s}

Table 3. Interfacial tension of PLA, PBS, and ZnO-NPs.

Where θ is the contact angle, ω is the wettability characteristic, γ_{s1} is the interfacial energy between the solid particle and polymer 2, γ_{s2} is the interfacial energy between the solid particle and polymer 1, and γ_{12} is the interfacial tension of polymer 1 and 2, respectively.

To calculate the interfacial tension between the polymers and ZnO-NPs, we used the geometric equation of Owens and Vendet (Eq. 3)[38]. This equation is more suitable for systems consisting of a high-energy material, such as nanoparticles, and a low-energy material, such as a polymer:

$$\gamma_{12} = \gamma_1 + \gamma_2 - 2\sqrt{\gamma_1^d \gamma_2^d} - 2\sqrt{\gamma_1^p \gamma_2^p} \tag{3}$$

The interfacial tension between the polymer components was calculated using the mean harmonic (Eq. 4).

$$\gamma_{12} \equiv \gamma_1 + \gamma_2 - 4\left[\frac{\gamma_1^d \gamma_2^d}{\gamma_1^d + \gamma_2^d} + \frac{\gamma_1^p \gamma_2^p}{\gamma_1^p + \gamma_2^p}\right] \tag{4}$$

The surface tensions of components 1 and 2 are denoted as γ_1 and γ_2, respectively. The dispersive (γ_1^d) and polar (γ_1^p) surface energy components of polymer 1, and the corresponding components for polymer 2 (γ_2^d and γ_2^p) are provided in Table 2. The interfacial tensions between each system constituent were calculated and are shown in Table 3. These values were then used to calculate the wetting coefficient. According to Young's relation, the preferential location of nanoparticles is determined based on the calculated value.

In general, the three main factors that influence the placement of nanoparticles in a polymer blend are viscosity, surface tension, and interfacial tension.

$\omega_{12} > 1$: ZnO-NPs would preferentially distribute within the matrix phase (PLA).

$\omega_{12} < -1$: ZnO-NPs distributed within the dispersed phase (PBS).

$-1 \leq \omega_{12} \leq 1$: ZnO-NPs distribute at the interface.

The calculated surface tension for each component is described in Table 2:

By comparing the surface tension values of ZnO nanoparticles in the PLA matrix phase and the PBS dispersed phase, it is possible to predict the preferential positioning of the nanoparticles. Generally, nanoparticles tend to migrate toward the component with lower surface tension, resulting in enhanced interfacial adhesion between the phases[39].

Utilizing Eq. 1, the calculated value of $\omega_{12}$was determined to be 1.37. Given that this value exceeds 1, it is evident that ZnO nanoparticles are likely to be situated within the PLA.

The morphology of PLA/PBS blends (80/20 wt%) and their nanocomposites with ZnO-NPs, neat CS, P-CS-ZnO-NPs, and NF-CS-ZnO-NPs were analyzed using FE-SEM micrographs. Cryo-fractured surface micrographs of the studied samples are presented in Fig. 4. The droplet radius was determined by selecting 100 particles and calculating their average which the obtained results are presented in Table 4.

Figure 4(a) shows the PLA/PBS blend with PLA as the matrix and PBS as dispersed droplets (average radius 423 nm). Weak interfacial adhesion between PLA and PBS leads to the formation of circular voids, indicating poor dispersion of PBS within the PLA matrix[40,41].

Figure 4(b) shows the PLA/PBS blend containing neat CS. Although some voids are visible, the addition of CS appears to improve the compatibility between the two phases, resulting in stronger interfacial adhesion between the dispersed droplets and the matrix. This enhancement is likely due to interactions between the polar groups of CS and the ester bonds of both polymers, leading to better phase adhesion and a more uniform morphology. The fracture surface also suggests noticeable improvements.

Figure 4(c) presents the PLA/PBS/ZnO 0.1 wt% nanocomposite (ZnO-0.1), where the incorporation of ZnO nanoparticles reduced the PBS domain size to 408 nm. A finer morphology with higher interfacial adhesion is also evident. This suggests that ZnO alters the morphology, possibly by promoting PBS droplet breakup or acting as defect sites. Furthermore, interactions among functional groups induced by ZnO addition may also contribute to the finer morphology observed in this sample.

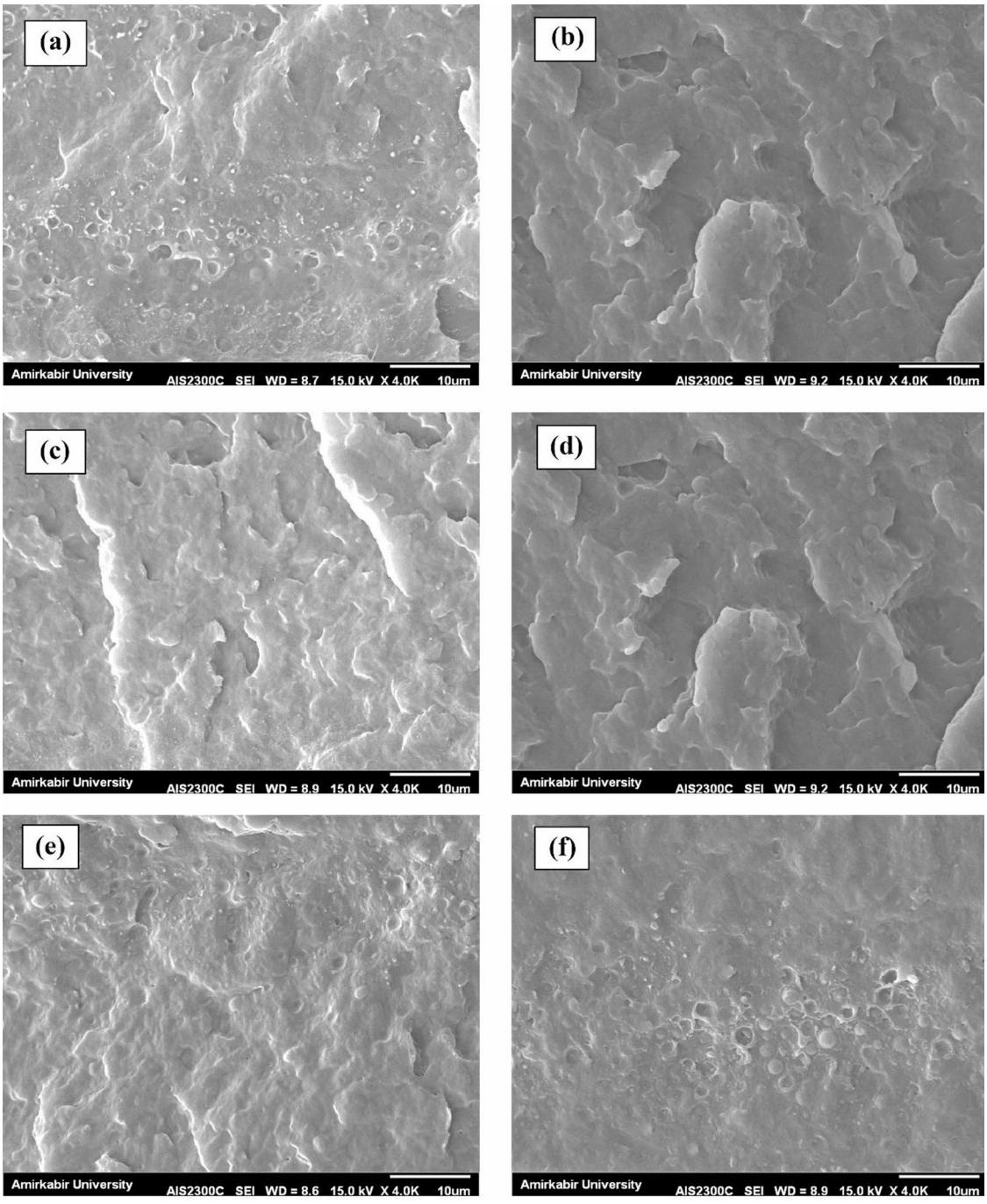

Fig. 4. FE-SEM images of (**a**) PLA/PBS, (**b**) PLA/PBS/CS, (**c**) ZnO 0.1, (**d**) ZnO-CS-F 0.1, (**e**) ZnO-CS-F 0.25, (**f**) ZnO-CS-F 0.5.

Sample	Average radius of PBS (nm)
PLA/PBS	423
ZnO 0.1	408
ZnO-CS-F 0.1	379
ZnO-CS-F 0.25	349
ZnO-CS-F 0.5	395

Table 4. Average radius of PLA/PBS, and its nanocomposites.

Figures 4(d–f) display PLA/PBS blends containing nanohybrids at 0.1, 0.25, and 0.5 wt% loadings. At 0.1 wt%, the PBS domain size decreased to 379 nm, indicating partial compatibilization of the two phases through nanohybrid incorporation. At 0.25 wt%, the domain size reached a minimum of 349 nm, with no visible voids. This improvement can be attributed to the combined effects of polar interactions between CS and the PLA/PBS phases, the kinetic inhibition of droplet coalescence by the nanohybrids, and the moderating effect of CS on ZnO activity—all of which reduce phase separation and maximize the beneficial influence of ZnO on morphology. Consequently, smaller dispersed PBS droplets and enhanced interfacial adhesion are achieved.

However, at 0.5 wt% loading, the PBS domain size increased to 395 nm, and voids reappeared, likely due to nanohybrid aggregation. This aggregation is attributed to the higher concentration of nanohybrids with large surface areas and the dominant degradative effect of the hybrids at elevated loadings.

Viscoelastic properties

Rheology, as a promising tool to analyze the microstructure, can be useful even in complex systems where the multiple sources of elasticity are present. Rheological observations can serve as an effective method to decouple these properties and analyze the microstructure[8,42–46]. In this context, Fig. 5 presents the rheological properties of PLA/PBS blends and their nanocomposites containing nano-hybrids with CS having fibrillar structure in the linear viscoelastic region. It should be noted that, due to the similar trends observed for both fibrillar and powdered CS, only the results for fibrillar CS are shown. Figure 5(a) illustrates the complex viscosity of the samples. The virgin PLA/PBS blend exhibits higher complex viscosity than that of nanocomposites, likely due to the dominant influence of nanoparticles (NPs) in reducing the viscosity. It can be noted that, incorporating 0.1 wt% ZnO into PLA/PBS sharply decreases complex viscosity; this can be attributed to the ZnO's catalytic role in accelerating degradation of biodegradable polymers like PLA and PBS, promoting chain scission, which is consistent with prior studies[23]. In contrast, hybridization of ZnO with CS (ZnO-CS-F 0.1) interestingly increased the complex viscosity compared to pure ZnO at the same concentration[47]. This enhancement suggestively originates from the improved NP dispersion by CS, reduced ZnO content in the hybrid, and possibly mitigating the degradation or higher influence on the movement of polymer chains as a consequence of higher interaction or engagements. It needs more investigations, which will be discussed in the following. However, increasing the ZnO-CS concentration from 0.1 to 0.5 wt% resulted in a decrease in the complex viscosity, reflecting higher ZnO content and intensified degradation[23].

Figures 5(b) and 5(c) show the storage modulus (G′) and loss modulus (G″) versus frequency, respectively, mirroring the complex viscosity trends. The PLA/PBS blend exhibits higher moduli, which were decreased with ZnO addition and partially recovered with ZnO-CS hybrids at low concentrations, before declining at higher hybrid loadings due to degradation.

Figure 5(d) presents Han plots (log G′ vs. log G″), which can be used to assess the polymer blend miscibility and nanocomposite elasticity. For fully miscible systems, the slope at low frequencies is 2, but immiscibility reduces this slope[48]. The PLA/PBS blend deviates from a slope of 2, indicating partial immiscibility. Adding 0.1 wt% ZnO further decreased the slope, reflecting reduced elasticity due to degradation, as observed in viscosity and moduli. Incorporating 0.1 wt% ZnO-CS hybrid increased the slope compared to pure ZnO, suggesting enhanced elasticity due to CS-mediated dispersion and lower ZnO activity. However, at 0.5 wt% ZnO-CS, the slope decreased monotonically, aligning with the viscosity and moduli trends, as increased ZnO content accelerates the degradation.

Figure 5(e-f) displays the relaxation spectra of the prepared blend and nanocomposites, revealing two distinct peaks for the virgin PLA/PBS blend: one at low relaxation times (related to the relaxations of chains of polymers) and another at higher relaxation times (corresponding to the relaxation of dispersed droplets), confirming phase immiscibility[23]. Adding 0.1 wt% ZnO reduces both peak intensities, suggesting ZnO acts as a powerful degrading agent that notably decreases the molecular weight of both polymers. Interestingly, a tail at high relaxation times is observed, which is usually correlated to the relaxation of chains located at the interface[23]. It can be ascribed to the interaction of degraded polymer chains of both types, which suggestively possess some functional groups as a consequence of degradation[23]. At 0.1 wt% NF-ZnO-CS, the polymer chain's peak disappears, and the droplet relaxation's peak persists with reduced intensity in association with no tail, indicating mitigated degradation compared to pure ZnO in the case of droplets that are relatively diluted with nanoparticles and lower interaction in the interphase region, as discussed above[4,43,47].

At 0.25 wt% NF-ZnO-CS, both peaks nearly disappear while the interfacial peak becomes more pronounced, indicating intensified PLA degradation, as expected. At 0.5 wt% NF-ZnO-CS, the relaxation spectrum becomes featureless with low overall intensity and a highly intensified tail peak, reflecting the severe degradative effect of the added nanohybrid, which generates low-molecular-weight fragments and strong interfacial interactions[4]. Interestingly, the behavior and relaxation spectra of ZnO-CS-F 0.1 and ZnO-CS-F 0.5 are relatively similar, suggesting that hybridization provides significantly greater control—by approximately five orders of magnitude—over the degradative activity of ZnO.

Mechanical properties

The tensile properties of PLA/PBS blends and their nanocomposites, including ZnO-NPs, NF-CS-ZnO-NPs, and P-CS-ZnO-NPs, were evaluated to assess the mechanical performance of the samples, as shown in Fig. 6. The stress–strain curve of the ZnO-CS-F 0.5 sample is shown in Fig. 6(a) as a representative example. Mechanical tests were repeated five times for each sample, and the results exhibited only minor variations, demonstrating good reproducibility and reliability.

The results, such as tensile strength, tensile modulus, and elongation at break, are shown in Fig. 6 (b).

According to Fig. 6(b), pure PLA displays high tensile strength (50.5 ± 2.5 MPa) and modulus (1299.2 ± 64.9 MPa) but low elongation at break (14.01 ± 0.7%) due to its brittle nature. Pure PBS exhibits

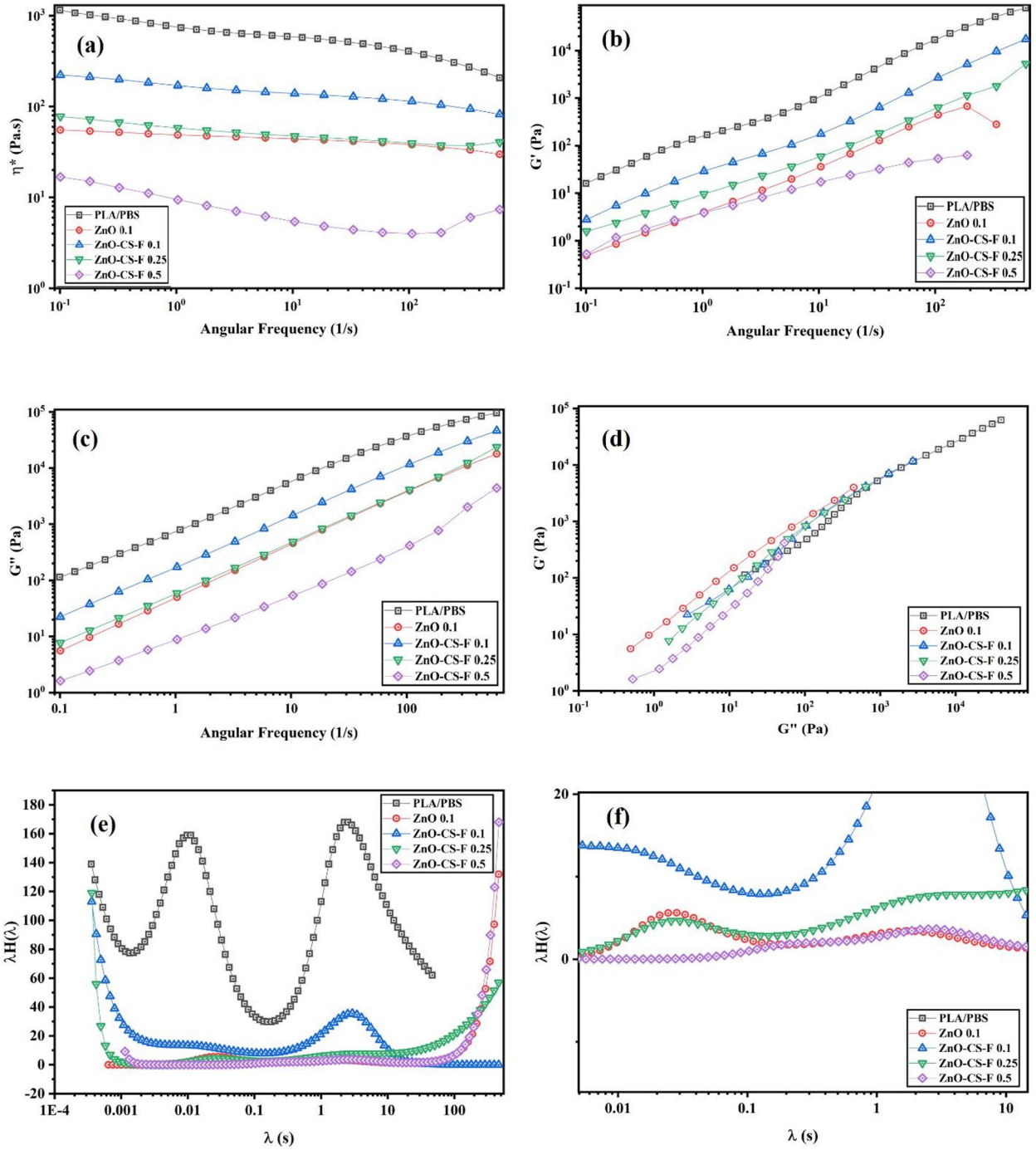

Fig. 5. Plots showing (**a**) complex viscosity, (**b**) storage modulus, (**c**) loss modulus as a function of frequency, (**d**) Han plots, (**e**) relaxation spectra, and (**f**) the magnified view of the relaxation spectra for PLA/PBS, ZnO (0.1 wt%), ZnO–CS-F (0.1 wt%), ZnO–CS-F (0.25 wt%), and ZnO–CS-F (0.5 wt%) samples.

lower strength (20.3 ± 1.01 MPa) and modulus (265 ± 13.2 MPa) but higher elongation (58 ± 2.9%), reflecting its ductility. The PLA/PBS blend (20 wt% PBS) balances these properties with tensile strength (32.1 ± 1.6 MPa), modulus (1184.2 ± 59.2 MPa), and increased elongation (24.4 ± 1.2%). This added flexibility, at the expense of reduced strength and modulus, comes from PBS's properties, although imperfect PLA/PBS compatibility limits the mechanical synergy.

Incorporating 0.1 wt% of ZnO-NPs significantly reduced the tensile strength (14 MPa), modulus (731.9 MPa), and elongation (2.5%), suggestively attributed to a significant degrading role of ZnO nanoparticles[49].

ZnO-NPs acted as a degrading catalyst and caused chain scission, reducing molecular weight and entanglement, which worsened mechanical properties. This aligns with relaxation spectrum data, where the suppression of PLA and PBS relaxation modes indicates impaired chain mobility without effective reinforcement[4].

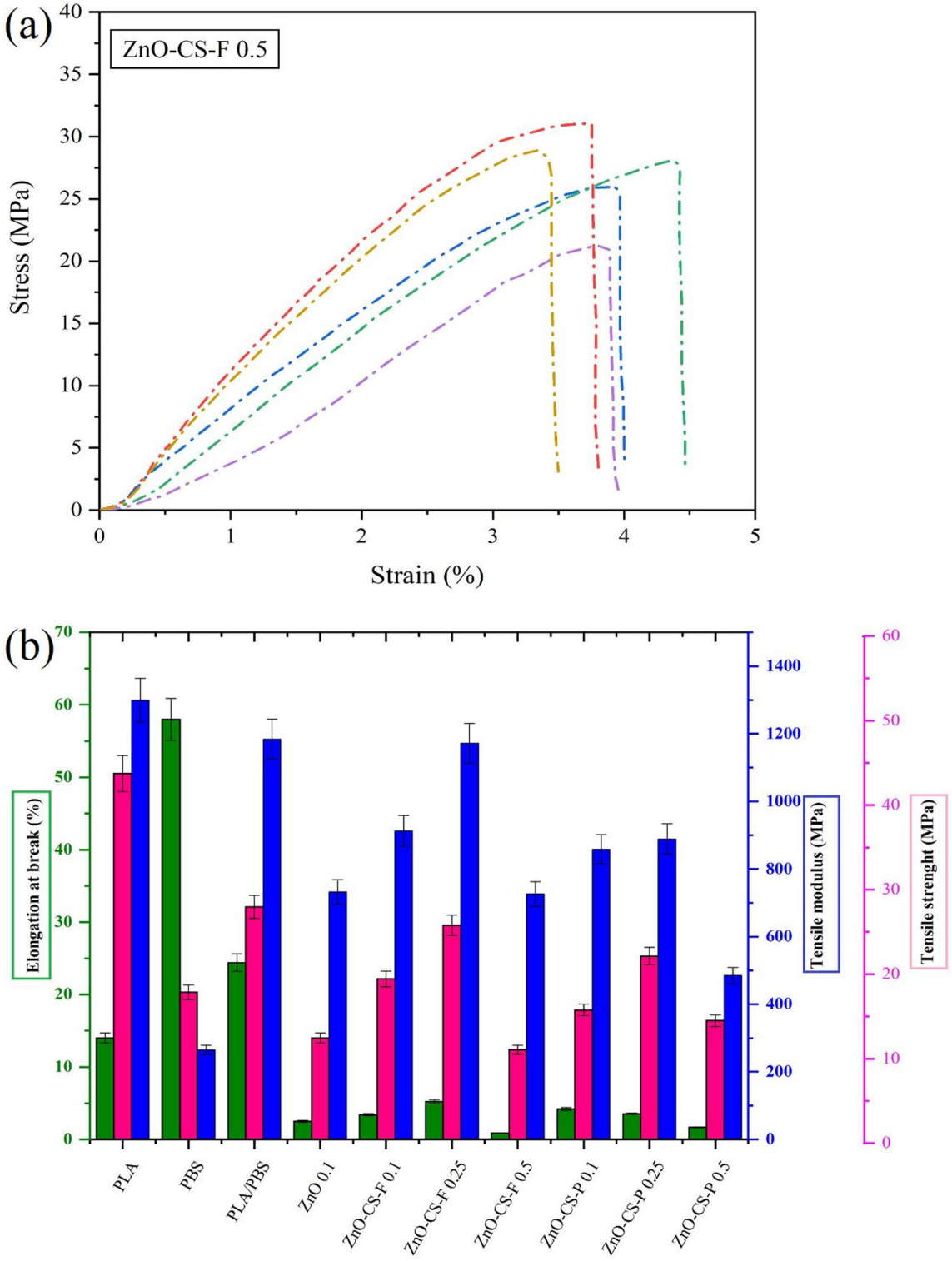

Fig. 6. Plots showing (**a**) the stress–strain curve of the ZnO-CS-F (0.5 wt%) sample and (**b**) the mechanical properties of PLA/PBS nanocomposites incorporating ZnO nanoparticles, NF-CS-ZnO nanohybrids, and P-CS-ZnO nanohybrids at filler loadings of 0.1, 0.25, and 0.5 wt%.

Mechanical studies show that hybridizing ZnO with CS, particularly in fibril form (NF-CS-ZnO), enhances tensile performance. This improvement likely arises from the smaller size of the synthesized ZnO particles and their better dispersion, together with the positive role of CS in compatibilizing the two phases. As a result, interfacial adhesion and overall mechanical strength are improved. Notably, at 0.1 wt%, the mechanical properties recover significantly, while at 0.25 wt% nanohybrid loading, the tensile strength (29.5 MPa) and

modulus (1172.1 MPa) approach those of the neat PLA/PBS blend. This enhancement is likely due to more efficient stress transfer across the PLA/PBS interface.

This behavior also correlates with the interface-related relaxation observed in the relaxation spectrum (Fig. 5e), indicating effective interfacial bridging by the hybrid and a well-balanced interaction between the synthesized ZnO and the functional groups of the polymer chains—both influenced by controlled degradation. However, at 0.5 wt%, the mechanical performance declines sharply, likely due to particle aggregation or the formation of a rigid, percolated network. Additionally, the increasing degradative effect of ZnO at higher loadings contributes to greater brittleness and chain scission, leading to inferior mechanical performance, as evidenced by the nearly flat relaxation spectrum. This observation is consistent with the morphological findings.

It is worth noting that nanocomposites containing powdered CS-ZnO hybrids (P-CS-ZnO) exhibited a similar trend but showed lower tensile strength and modulus at all concentrations compared to the NF-CS-ZnO systems. The enhanced surface area and physical entanglement of the fibrillar CS likely promote better stress distribution and phase compatibility, resulting in superior performance relative to the powdered form.

In summary, the mechanical properties closely follow the trends seen in the relaxation spectrum and further support the morphological analysis: an optimal ZnO-CS hybrid concentration (0.25 wt%, especially in fibrillar form) improves the mechanical integrity by enhancing interfacial bonding, promoting more controlled synthesis of ZnO particles, and achieving better dispersion of ZnO, particularly at the interphase boundaries. Excessive loading (0.5 wt%) undermines the matrix cohesion, significantly decreasing mechanical performance due to aggregation and the marked degradation of chain dynamics.

Hydrolytic degradation properties

To investigate the hydrolytic degradation of the prepared samples, all films with identical dimensions were placed separately in the containers containing 10 mL of 1 molar sodium hydroxide (NaOH) at room temperature. After 42 h, their weight changes were examined. At the end of the specified period, the samples were removed from the NaOH solution, thoroughly washed with distilled water, and completely dried to assess their weight variations. The weight loss of the samples relative to their initial weight was analyzed and plotted as a function of nanoparticle concentration in Fig. 7(a). Additionally, photographs of all samples were taken after the completion of the test (Fig. 7(b)) to visually assess the extent of physical degradation. Samples containing higher amounts of nanohybrids showed more pronounced degradation, with noticeable rupture and shrinkage compared to the pure or lower-loading samples.

A gradual increase in the degradation rate was observed with the incorporation of ZnO and NF-CS-ZnO hybrids[50]. The neat PLA/PBS blend exhibited the lowest mass loss, while the addition of 0.1 wt% ZnO nanoparticles slightly accelerated the degradation[23]. This effect became more pronounced with the inclusion of NF-CS-ZnO hybrids at 0.1%, 0.25%. It reached a maximum at 0.5%, indicating a clear concentration-dependent enhancement for the case of hydrolytic degradation. The PLA/PBS blend exhibited minimal mass loss, attributed to the hydrolytic stability of PLA and PBS in neutral aqueous environments[10]. It can be deduced that limited miscibility between PLA and PBS restricts water uptake at phase boundaries, reducing ester bond cleavage and consequently lowering degradation. Incorporating 0.1 wt% ZnO-NPs increased mass loss, likely due to ZnO's amphoteric nature, creating localized pH changes that accelerate ester hydrolysis[23].

Improved ZnO dispersion through hybridization with chitosan (CS), as confirmed by SEM micrographs, enhanced the reactive surface area available for degradation. At 0.25 wt%, the nanocomposite exhibited higher mass loss, attributed to an increased interfacial area and optimal filler dispersion, characterized by 349 nm PBS domains. This composition achieved a balanced interaction between ZnO and the polymer matrix, resulting in the best overall performance among the studied samples. In this specific case, the combination of the nanohybrid amount and its distinct morphology established an equilibrium between water diffusion resistance, polymer chain dynamics, phase compatibility, and the degradability of ZnO within the nanohybrid. This balance also corresponds to the observed enhancement in tensile strength (29.5 MPa), indicative of improved interfacial compatibility.

At 0.5 wt%, the highest mass loss was recorded, suggesting a threshold beyond which excessive hydrophilic domains, elevated ZnO content, and possible nanohybrid aggregation (395 nm PBS domains) promote accelerated degradation. These conditions may lead to the formation of micro-cracks or voids, as observed in Fig. 4(f), acting as water channels that expedite hydrolysis but compromise mechanical integrity (12.3 MPa). Overall, the results indicate that ZnO catalyzes hydrolysis, while CS enhances matrix permeability; when both are present at high concentrations, their synergistic effect intensifies degradation.

These findings emphasize the crucial role of filler chemistry and morphology in governing the degradation kinetics. The NF-CS-ZnO nanohybrids at 0.25 wt% achieve an optimal balance between interfacial compatibility and controlled degradation, demonstrating potential for tunable biodegradability in environmentally responsive applications. Further investigation into the degradation products and water absorption behavior could provide a more systematic understanding of these mechanisms.

DFT simulation

To verify the experimental findings, density functional theory (DFT) calculations were conducted to evaluate the molecular interactions between the main components of the system: PLA, PBS, ZnO nanoparticles, and CS. The total binding energies of various binary and ternary complexes were determined using optimized geometries, providing valuable insights into the thermodynamic favorability of each interaction. The molecular structures of PLA, PBS, ZnO, and CS used in this DFT calculation are shown in Fig. 8. The obtained results can be observed in Fig. 9.

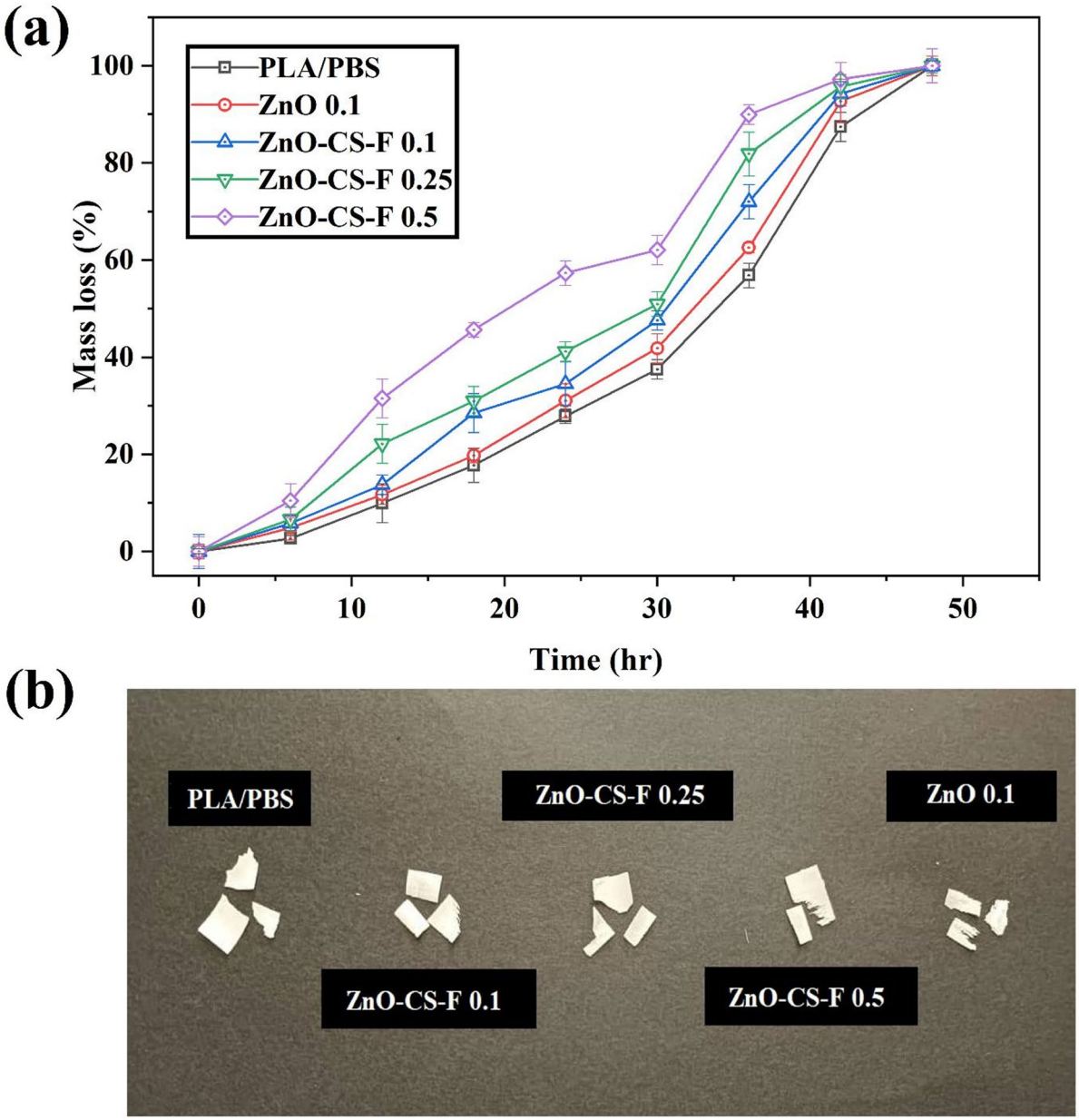

Fig. 7. Figure showing (**a**) the mass loss of the PLA/PBS blend and its nanocomposites containing ZnO and NF-CS-ZnO nanohybrids at 0.1, 0.25, and 0.5 wt% after 42 h of exposure to 1 M sodium hydroxide (NaOH) at room temperature, and (**b**) images illustrating the physical degradation of the PLA/PBS blend and the corresponding nanocomposites incorporating ZnO nanoparticles and NF-CS-ZnO nanohybrids under identical conditions.

Intermolecular affinity and binding energies Among the binary systems, PLA–ZnO and PBS–ZnO showed the most negative binding energies, at − 856.7 kJ/mol and − 391.6 kJ/mol, respectively. These highly favorable values indicate strong interactions between the metal oxide nanoparticles and the polymer backbones, suggesting potential for improved compatibility and dispersion when ZnO is added to the PLA/PBS matrix. In contrast, the PLA–CS complex produced a slightly positive binding energy (+ 20.4 kJ/mol). The positive binding energy obtained for the PLA–CS complex indicates that the interaction between these two polymers is thermodynamically unfavorable, meaning that the separated components are energetically more stable than the bound configuration. This result reflects the well-known incompatibility between PLA and CS, which arises primarily from their polarity mismatch—PLA being relatively hydrophobic due to its aliphatic polyester backbone, and CS being highly hydrophilic with abundant amino and hydroxyl functional groups. The lack of strong interfacial interactions such as hydrogen bonding or dipole–dipole attraction results in poor interfacial adhesion and high interfacial energy, leading to phase separation. Similar behavior has been experimentally reported by Wan et al. (2006)[51], who observed weak interactions and pronounced phase separation in PLA/CS blends. Furthermore, computational studies by Santos et al. (2025)[52] demonstrated that chemical functionalization of chitosan (e.g.,

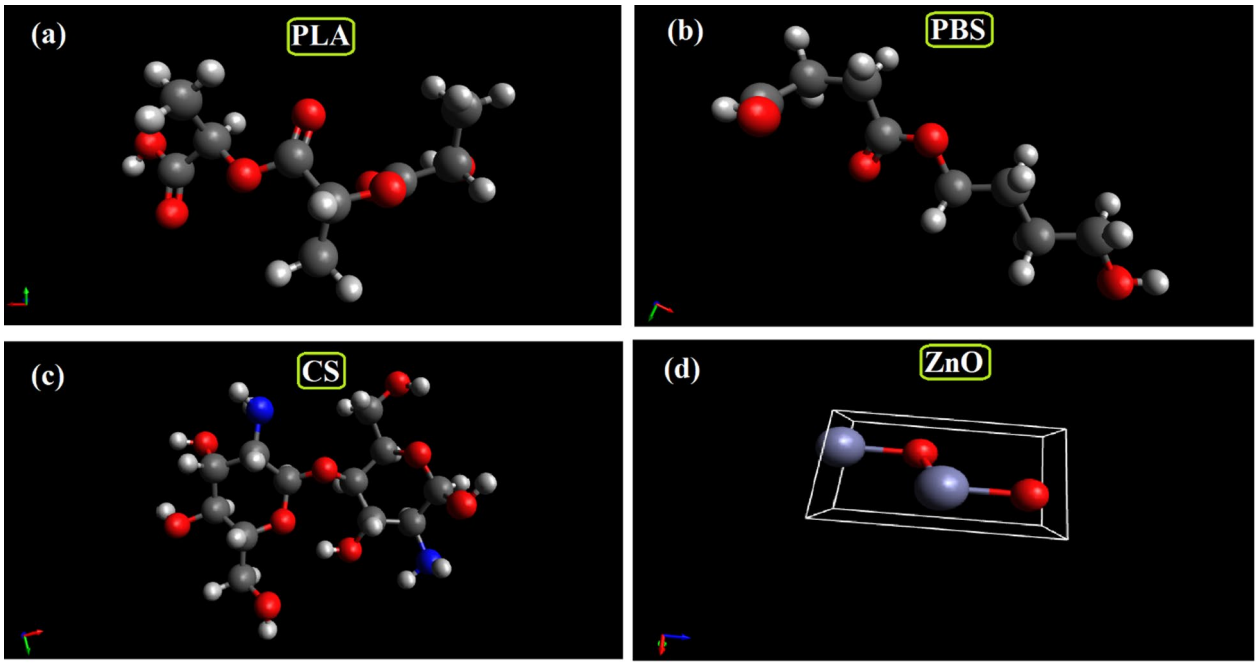

Fig. 8. Gaussian molecular structures of (**a**) PLA, (**b**) PBS, (**c**) CS, and (d) ZnO chemical structures.

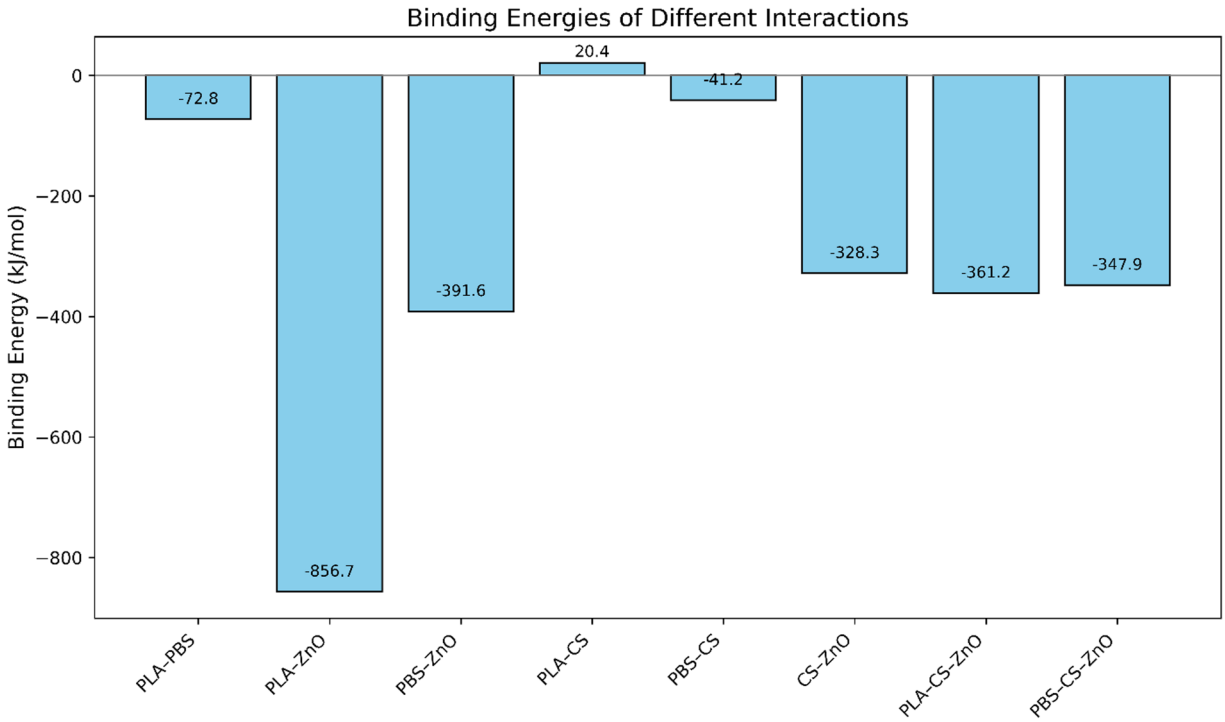

Fig. 9. Bar chart showing the binding energies of binary and ternary complexes involving PLA, PBS, ZnO, chitosan (CS), and CS–ZnO hybrids, as calculated using Density Functional Theory (DFT).

with amino acids) substantially improves its binding affinity with hydrophobic systems, further confirming that native chitosan lacks the necessary functional groups for effective interaction with PLA. These findings collectively support our computational and experimental observations that hybridization of CS with ZnO significantly improves compatibility by introducing new active sites that facilitate stronger interfacial bonding with PLA.

Interestingly, the ternary PLA–CS–ZnO and PBS–CS–ZnO systems displayed binding energies of − 361.2 kJ/mol and − 347.9 kJ/mol, respectively. These results indicate that ZnO plays a critical compatibilizing role

by stabilizing the interaction between the polymers and CS, effectively reducing the interfacial energy and enhancing thermodynamic compatibility. This bridging effect is likely due to the ability of ZnO to form coordination bonds and hydrogen bonds with both the polar groups on CS and the ester/carbonyl functionalities on PLA and PBS[53,54].

Morphological evidence of improved interfacial compatibility Experimental morphological analysis using microscopy revealed notable changes in the microstructure of the PLA/PBS blends upon incorporation of ZnO and CS-based nanohybrids. In the unmodified blend, clear phase separation and poor interfacial adhesion were observed, consistent with the weak interaction predicted for PLA–CS in DFT results. Upon addition of ZnO and especially ZnO–CS hybrids, phase dispersion became more uniform, and the size of PBS domains decreased, indicating improved interfacial compatibility. These microstructural improvements correspond well with the increased binding energies observed in the ternary complexes from DFT analysis.

Rheological correlation with molecular interactions The relaxation spectrum of the blends showed two distinct peaks in the base PLA/PBS system, representing different relaxation modes of the two polymers and dispersed phase, along with a tail indicating the interphase region. The addition of ZnO nanoparticles caused a significant decrease in peak intensity and even the disappearance of one peak, suggesting improved compatibility and less phase separation, as well as stronger interactions among chains at the interface. These changes are consistent with the DFT-predicted strong PLA–ZnO and PBS–ZnO interactions, which would help improve stress transfer and chain mobility across the interface, thus changing the viscoelastic behavior of the blend.

When ZnO–CS nanohybrids were introduced, the relaxation spectra further confirmed improved miscibility, especially at low concentrations (0.1–0.25 wt%). At higher hybrid content (0.5 wt%), the peaks nearly disappeared, indicating network disruption or excessive plasticization, which aligns with the moderate but still favorable binding energy observed for the PLA–CS–ZnO and PBS–CS–ZnO systems.

Mechanical properties and their energetic basis The mechanical performance of the composites also aligned well with DFT findings. Samples with ZnO and ZnO–CS hybrids exhibited increased strength and modulus at low to moderate filler concentrations, due to improved interfacial adhesion and load transfer efficiency. The strong binding energies (especially for PLA–ZnO and the ternary complexes) indicate robust interactions that limit the mobility of polymer chains, leading to higher stiffness. At higher hybrid loadings, mechanical properties decreased, likely because of agglomeration or over-degradation, which is reflected in the reduced net interaction energy and the broader, weaker intermolecular network.

Hydrolytic degradation and interfacial dynamics Mass loss studies under hydrolytic conditions showed a clear trend of increasing degradation with the addition of ZnO and ZnO–CS nano-hybrids. This behavior is supported by DFT results, which suggest that ZnO establishes strong interactions with both polymers and CS, thereby promoting higher interfacial activity. These enhanced interfacial interactions likely increase the local hydrophilicity and create micro-domains of greater water susceptibility, facilitating hydrolytic attack. The increase in degradation rate with rising hybrid content (0.1 to 0.5 wt%) is therefore consistent with a combination of energetic affinity and morphological disruption observed both computationally and experimentally.

This study distinguishes itself from previous works by demonstrating a novel, non-grafted CS–ZnO hybrid compatibilizer that simultaneously enhances mechanical performance, morphological uniformity, and degradation behavior of PLA/PBS blends at low filler concentrations. Unlike many prior studies that examine chitosan or ZnO separately or rely on chemical grafting, this work provides combined experimental and theoretical insights into the interfacial synergy of CS–ZnO nanohybrids.

Conclusion

This study demonstrates that incorporating CS–ZnO nano-hybrids into PLA/PBS (80/20 wt%) blends significantly enhances mechanical performance, phase compatibility, and rheological behavior. At only 0.25 wt% loading, CS–ZnO improved tensile strength and Young's modulus, while SEM analysis revealed finer phase dispersion and reduced interfacial discontinuities. Rheological data indicated stronger chain interactions and enhanced network formation in the molten state, corroborated by relaxation spectra.

Hydrolytic degradation studies showed accelerated and controlled breakdown of the nanocomposites, providing a functional advantage for sustainable applications. DFT simulations further confirmed the synergistic role of ZnO as a molecular bridge, enhancing PLA–chitosan compatibility and supporting experimental findings.

This work introduces a novel multifunctional compatibilizer (CS–ZnO) that simultaneously strengthens the matrix, improves phase adhesion, and modulates degradation, achieving significant improvements at very low filler content. These advancements position PLA/PBS/CS–ZnO nanocomposites as promising candidates for sustainable packaging, biomedical devices, and other high-value applications, while future work will explore scalable processing and long-term environmental performance.

Data availability

The data that support the findings of this study are available from the corresponding author upon reasonable request.

Received: 16 September 2025; Accepted: 22 October 2025
Published online: 24 November 2025

References

1. Oliver-Cuenca, V. et al. Bio-Based and biodegradable polymeric materials for a circular economy. *Polym. (Basel)*. **16**, 3015 (2024).
2. Liu, Y-Y. & Echeverry-Rendón, M. 3D-printed biodegradable polymer scaffolds for tissue engineering: an overview, current stage and future perspectives. *Next Mater.* **8**, 100647 (2025).
3. Oladele, I. O. et al. Current application of recycled waste plastics as a sustainable materials: A review on availability, processing and application. *J. Thermoplast Compos. Mater.* **38**, 277–301 (2025).
4. Khaleghi, R., Dadashi, P. & Babaei, A. Investigating the Effect of GO-ZnO nano-hybrid on the mechanical, rheological, and Degradation Performance of Poly (butylene succinate). *Polym. Compos* (2024).
5. Dehghan, F., Dadashi, P., Babaei, A. & Partovi, R. Biodegradable PLA films incorporating GO-ZnO hybrid and Mentha longifolia oil: Fabrication and characterization. *Polym. Eng. Sci.* (2025).
6. Kumar, K. S. & Singh, I. Sustainable oxalic acid treatment of lignocellulosic fibers for ensuring improved performance of treated fibers based bio PBS composites. *Int. J. Biol. Macromol.* **294**, 139507 (2025).
7. Yan, T., Chen, K., Wang, X. & Qiao, Y. Development of CS/PLA composites with enhanced ductility via PBS elastomer reinforcement. *Int. J. Mol. Sci.* **26**, 4643 (2025).
8. Haghgoo, G., Dadashi, P. & Babaei, A. Effects of cellulose nanocrystals localization on compatibility between polylactic acid and polycaprolactone: correlating the microstructure and mechanical performance. *Polym. Adv. Technol.* **36**, e70113 (2025).
9. Yokohara, T. & Yamaguchi, M. Structure and properties for biomass-based polyester blends of PLA and PBS. *Eur. Polym. J.* **44**, 677–685 (2008).
10. Su, S., Kopitzky, R., Tolga, S. & Kabasci, S. Polylactide (PLA) and its blends with Poly (butylene succinate)(PBS): A brief review. *Polym. (Basel)*. **11**, 1193 (2019).
11. Bhatia, A., Gupta, R. K., Bhattacharya, S. N. & Choi, H. J. Compatibility of biodegradable Poly (lactic acid)(PLA) and Poly (butylene succinate)(PBS) blends for packaging application. *Korea-Australia Rheol J.* **19**, 125–131 (2007).
12. Homklin, R. & Hongsriphan, N. Mechanical and thermal properties of PLA/PBS co-continuous blends adding nucleating agent. *Energy Procedia*. **34**, 871–879 (2013).
13. Ramesan, M. T. et al. Hydroxyapatite nanoparticles reinforced Polyvinyl alcohol/chitosan blend for optical and energy storage applications. *Polym. Eng. Sci.* **64**, 1378–1390 (2024).
14. Hunais, O. M. et al. Tuning the structural, mechanical, thermal and electrical properties of in-situ polymerized polyindole/carboxymethyl chitosan/nickel oxide blend nanocomposites for energy storage applications. *J. Polym. Environ.* **32**, 4035–4045 (2024).
15. Meera, K. & Ramesan, M. T. Performance of boehmite nanoparticles reinforced carboxymethyl chitosan/polyvinyl alcohol blend nanocomposites tailored through green synthesis. *J. Polym. Environ.* **31**, 447–460 (2023).
16. Meera, K. & Ramesan, M. T. Modulating the properties of carboxymethyl chitosan/polyethylene oxide nanocomposites with aluminium Oxy hydroxide: A comprehensive study. *Int. J. Biol. Macromol.* **282**, 137034 (2024).
17. Sankar, S., Krishnaraj, T. P., Sunojkumar, P. & Ramesan, M. T. Chitosan-functionalized Poly (thiophene-co-pyrrole) nanocomposites: promising materials for optoelectronics and antibacterial surfaces. *J. Mol. Liq.* **437**, 128319 (2025).
18. Meera, K. & Ramesan, M. T. Development of high-performance biopolymer nanocomposites derived from carboxymethyl chitosan/boehmite via green synthesis. *Polym. Compos.* **44**, 1135–1148 (2023).
19. Meera, K. & Ramesan, M. T. Tailoring the performance of boehmite nanoparticles reinforced carboxymethyl chitosan/cashew gum blend nanocomposites via green synthesis. *Polym. (Guildf).* **268**, 125706 (2023).
20. Zabihi, E. et al. Facile and rapid in-situ synthesis of chitosan-ZnO nano-hybrids applicable in medical purposes; a novel combination of biomineralization, ultrasound, and bio-safe morphology-conducting agent. *Int. J. Biol. Macromol.* **131**, 107–116 (2019).
21. Kannusamy, P. & Sivalingam, T. Chitosan–ZnO/polyaniline hybrid composites: polymerization of aniline with chitosan–ZnO for better thermal and electrical property. *Polym. Degrad. Stab.* **98**, 988–996 (2013).
22. Haldorai, Y. & Shim, J-J. Chitosan-zinc oxide hybrid composite for enhanced dye degradation and antibacterial activity. *Compos. Interfaces*. **20**, 365–377 (2013).
23. Ahmadzadeh, Y., Babaei, A. & Goudarzi, A. Assessment of localization and degradation of ZnO nano-particles in the PLA/PCL biocompatible blend through a comprehensive rheological characterization. *Polym. Degrad. Stab.* **158**, 136–147. https://doi.org/10.1016/j.polymdegradstab.2018.10.007 (2018).
24. Vigneshwaran, N. et al. Functional behaviour of polyethylene-ZnO nanocomposites. *J. Nanosci. Nanotechnol.* **8**, 4121–4126 (2008).
25. Li, J., Fan, H. & Jia, X. Multilayered ZnO nanosheets with 3D porous architectures: synthesis and gas sensing application. *J. Phys. Chem. C.* **114**, 14684–14691 (2010).
26. Bayindir Bilgic, M., Lacin, N. T., Berber, H. & Mansuroglu, B. In vitro evaluation of alpha-tocopherol loaded carboxymethylcellulose Chitosan copolymers as wound dressing materials. *Mater. Technol.* **34**, 386–393 (2019).
27. Muraleedaran, K. & Mujeeb, V. M. A. Applications of Chitosan powder with in situ synthesized nano ZnO particles as an antimicrobial agent. *Int. J. Biol. Macromol.* **77**, 266–272 (2015).
28. Shafiq, M., Yasin, T., Aftab Rafiq, M. & Shaista Structural, thermal, and antibacterial properties of chitosan/ZnO composites. *Polym. Compos.* **35**, 79–85 (2014).
29. Zhao, S., You, B. & Jiang, L. Oriented assembly of zinc oxide mesocrystal in Chitosan and applications for glucose biosensors. *Cryst. Growth Des.* **16**, 3359–3365 (2016).
30. AbdElhady, M. M. Preparation and characterization of chitosan/zinc oxide nanoparticles for imparting antimicrobial and UV protection to cotton fabric. *Int J Carbohydr Chem* **2012**, 840591 (2012).
31. Magesh, G. et al. Tuning effect of polysaccharide Chitosan on structural, morphological, optical and photoluminescence properties of ZnO nanoparticles. *Superlattices Microstruct.* **117**, 36–45 (2018).
32. Saboor, A., Shah, S. M. & Hussain, H. Band gap tuning and applications of ZnO nanorods in hybrid solar cell: Ag-doped verses Nd-doped ZnO nanorods. *Mater. Sci. Semicond. Process.* **93**, 215–225 (2019).
33. Raja, K. et al. Synthesis of structural and optical characterization of surfactant capped ZnO nanocrystalline. *Spectrochim Acta Part. Mol. Biomol. Spectrosc.* **136**, 155–161 (2015).
34. Zak, A. K. et al. Effects of annealing temperature on some structural and optical properties of ZnO nanoparticles prepared by a modified sol–gel combustion method. *Ceram. Int.* **37**, 393–398 (2011).
35. Yu, J., Li, C. & Liu, S. Effect of PSS on morphology and optical properties of ZnO. *J. Colloid Interface Sci.* **326**, 433–438 (2008).
36. Revathi, T. & Thambidurai, S. Immobilization of ZnO on Chitosan-Neem seed composite for enhanced thermal and antibacterial activity. *Adv. Powder Technol.* **29**, 1445–1454 (2018).
37. Wu, D., Zhang, Y., Zhang, M. & Yu, W. Selective localization of multiwalled carbon nanotubes in Poly (ε-caprolactone)/polylactide blend. *Biomacromolecules* **10**, 417–424 (2009).
38. Wu, D. et al. Interfacial properties, viscoelasticity, and thermal behaviors of Poly (butylene succinate)/polylactide blend. *Ind. Eng. Chem. Res.* **51**, 2290–2298 (2012).
39. Torchinsky, I. & Rosenman, G. Wettability modification of nanomaterials by low-energy electron flux. *Nanoscale Res. Lett.* **4**, 1209–1217 (2009).
40. Saeed Ullah, M. et al. Miscibility and phase behavior of reactively compatibilized poly(lactic acid)/poly(butylene succinate) bio-blends using various rheological analyses. *J. Appl. Polym. Sci.* **140** https://doi.org/10.1002/app.54424 (2023).

41. Gu, Z. et al. Extraordinary toughness and heat resistance enhancement of biodegradable PLA/PBS blends through the formation of a small amount of interface-localized stereocomplex crystallites during melt blending. *Polym. (Guildf).* **262**, 125454 (2022).
42. Dadashi, P., Babaei, A. & Rostami, A. A new modified emulsion model for immiscible binary polymeric blends containing nanoparticles distributed in droplets. *Iran. J. Polym. Sci. Technol.* **34**, 83–94. https://doi.org/10.22063/jipst.2021.1795 (2021).
43. Elhamnia, M., Dadashi, P. & Motlagh, G. H. Investigating competition of strong interfacial interaction and chain scission in PBAT/EVOH/GO composite by rheological measurements. *J. Reinf. Plast. Compos.* **42**, 2381–2395 (2024).
44. Dadashi, P., Ray, S. S. & Babaei, A. Effect of graphene oxide localization on morphology development and rheological and mechanical properties of Poly(Lactic Acid)/Ethylene vinyl alcohol copolymer blend composites: A comprehensive study. *Polym. (Basel).* **16**, 1061. https://doi.org/10.3390/polym16081061 (2024).
45. Dadashi, P., Soltani, E., Elhamnia, M. & Motlagh, G. H. Decoupling interfacial compatibilization and chain extension in polymer blends using rheology: PBAT/EVOH with MDI. *J. Polym. Res.* **32**, 32 (2025).
46. Sadri, S. A. et al. Investigating compatibilization of polyoxymethylene/styrene-butadiene-styrene immiscible blend through addition of hydroxylated graphene. *Sci. Rep.* **14**, 24734 (2024).
47. Dadashi, P., Babaei, A. & Abdolrasouli, M. H. Investigating the hydrolytic degradation of PLA/PCL/ZnO nanocomposites by using viscoelastic models. *Polym. Eng. Sci.* **62**, 869–882. https://doi.org/10.1002/pen.25893 (2022).
48. Soltani, E., Motlagh, G. H., Elhamnia, M. & Dadashi, P. Highly efficient reactive compatibilization of biodegradable PBAT/EVOH blend by pMDI. *J. Appl. Polym. Sci.* e55666 (2024).
49. Rahman, M. M., Islam, M. S. & Li, G. S. Development of PLA/CS/ZnO nanocomposites and optimization its mechanical, thermal and water absorption properties. *Polym. Test.* **68**, 302–308 (2018).
50. Dadashi, P., Torbatinejad, K. & Babaei, A. Hybridization as a promising approach to engineering the desired performance of bio-nanocomposites: GO-ZnO hybrid reinforced PCL. *Sci. Rep.* **15**, 1–15 (2025).
51. Wan, Y., Wu, H., Yu, A. & Wen, D. Biodegradable polylactide/chitosan blend membranes. *Biomacromolecules* **7**, 1362–1372 (2006).
52. Santos, J. R. C., Abreu, P. E. & Marques, J. M. C. Towards nature-inspired materials for adsorbing pesticides: a multi-stage computational approach. *Phys. Chem. Chem. Phys.* **27** (2025).
53. Chong, W. J. et al. Biodegradable PLA-ZnO nanocomposite biomaterials with antibacterial properties, tissue engineering viability, and enhanced biocompatibility. *Smart Mater. Manuf.* **1**, 100004 (2023).
54. Wang, Q. et al. Fabrication of Cu/ZnO-loaded Chitosan hydrogel for an effective wound dressing material to advanced wound care and healing efficiency after caesarean section surgery. *Int. Wound J.* **21**, e14366 (2024).

Author contributions

Parsa Dadashi: Writing – original draft, Visualization, Resources, Conceptualization. Rozgol Bonsale : Visualization, Resources, Conceptualization. Amir Babaei: Writing – review & editing, Visualization, Supervision, Resources, Project administration, Funding acquisition, Conceptualization.

Funding

This work has been funded by the University of Golestan.

Declarations

Competing interests

The authors declare no competing interests.

Additional information

Correspondence and requests for materials should be addressed to A.B.

Reprints and permissions information is available at www.nature.com/reprints.

Publisher's note Springer Nature remains neutral with regard to jurisdictional claims in published maps and institutional affiliations.